INTERNATIONAL ATOMIC ENERGY AGENCY
UNITED NATIONS EDUCATIONAL, SCIENTIFIC AND CULTURAL ORGANIZATION

NTERNATIONAL CENTRE FOR THEORETICAL PHYSICS
100 TRIESTE (ITALY) - P.O.B. 586 - MIRAMARE - STRADA COSTIERA 11 - TELEPHONES: 224281/2/3/4/5/6
CABLE: CENTRATOM - TELEX 460392 - I

H4.SMR/164 -21

WORKSHOP ON CLOUD PHYSICS AND CLIMATE

23 November - 20 December 1985

CLOUD AND PRECIPITATION PROCESSES
Part V

HAILSTONES AND HAILSTORMS

C. VALI

University of Wyoming
U.S.A.

LECTURE 5 HAILSTONES AND HAILSTORMS

References: Books by Sulakvelidze, Goldhale, etc. - 1970's
Am. Meteor. Soc. Monograph # 33 - late 1970's
"Hailstorms of the High Plains" Knight & Squires editors - 1982

Major characteristics of hailstones:
- rough outer surface, lobes
- "onion ring" layers of clear and opaque ice
- trapped water
- crystallite sizes
- isotope composition
- embryo of graupel or frozen drop.

From these characteristics some deductions can be made regarding conditions of growth (T, LWC, Z, droplet sizes).

Theory of hail growth – initial growth of embryo by riming; as fall-velocity and size increase rate of collection of LWC increases and not all droplets freeze but temperature of surface rises to 0°C, i.e. hailstone becomes "wet"; thermal balance set up between dissipation of heat to air and freezing of some of the collected water. Difficulties are in calculations of heat and vapor exchange and of fall-velocity for irregularly-shaped hailstone. Water shedding possible

Hailstorms:
"Multicell" and "Supercell" structures
Regions of hailstone growth – periphery of main updraft core.

Models: Dynamics
Hailstone growth in flow-field derived from observed Doppler radar data
Nested grids

2

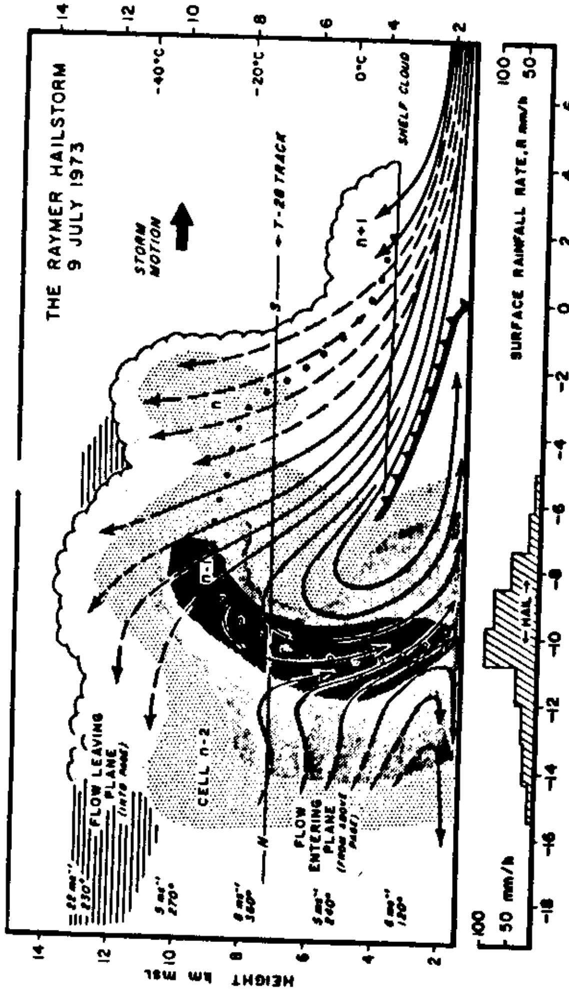

Figure 4.-- Descriptive model of a multicell thunderstorm in northeast Colorado, showing a vertical section along the direction of travel of the storm. Thick lines: smoothed streamlines of flow relative to moving storm; lightly stippled shading: extent of cloud; darker grades of shading: radar reflectivities of 35, 45, and 50 dBZ; open circle: trajectory of a hailstone during its growth from a small particle. (Right) temperature scale: temperature of a parcel lifted from the surface; (Left) velocities: environmental winds relative to the storm based on soundings behind the storm. The model can be regarded as an instantaneous view of a typical structure with four different cells (n + 1, n, n - 1, and n - 2) at different stages of evolution or it can be regarded as showing four stages in the evolution of an individual cell (Browning et al., 1976).

3

at altitudes ≥ 15 km throughout
...n. Also, infrared radiation (IR)
1980) indicate that cloud-top
as −66°C, a temperature found
profiles in Fig. 13.4. Thus, the in-
consistently penetrated some 2 to
...se height, which is shown to be

mountain ranges and foothills may have their ...

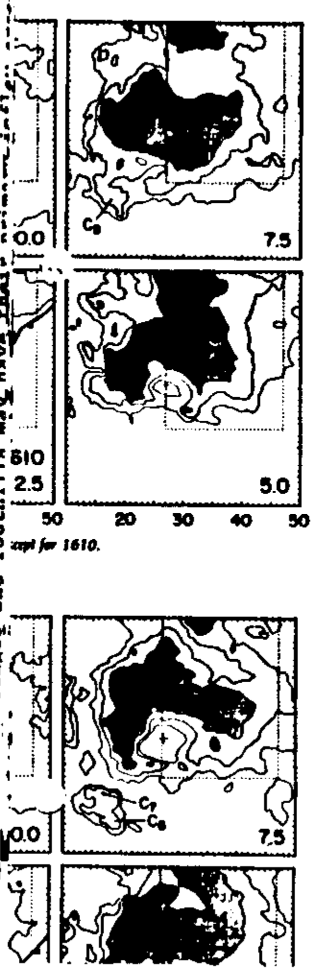

...cept for 1610.

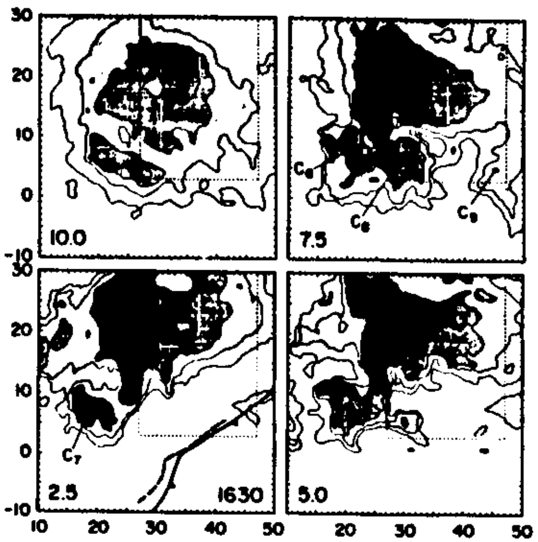

Figure 13.7e Same as Fig. 13.7a, except for 1630.

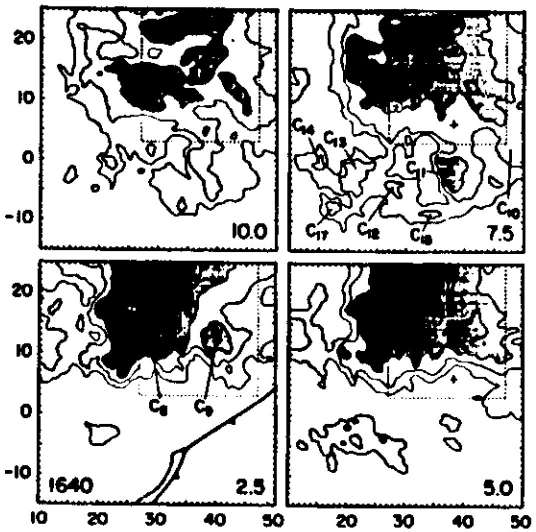

Figure 13.7f Same as Fig. 13.7a, except for 1640. Note shift in y coordinates.

Newton, Fankhauser 1975 4

Paragraph p747

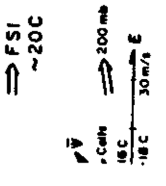

...f new cells with respect to centroid ...riangles denote those that at some ...osses, cells that formed outside the ...that separated from the north side ...orm location, the mean movement ...d arrows show storm-environment in the moist layer, 965–800 mb.

...hile dissipating. The general ...s on the north side, is like that ...ell cluster). This suggests that ...both the clusters and the cells ...noves over a swath to right of ...sters, while the clusters them... ...he mean wind as a result of

...f formation of new cells are ...e centroid (at *b*) of the 0–*db* ... of this storm (at maximum ...cally all new cells formed on ...ight). It is noteworthy that as ...he mean wind) as on the right ...d on the right side (triangles) ...ated the propagation process

... growth of the new cells on the upwind side (Fig. 7). The corresponding pattern is shown in Fig. 9 for a large multicellular storm described by HAMMOND [12], that moved strongly to the left of the wind. In this case, the mean cell movement was somewhat to left of the mean wind. Development of strong new cells predominantly occurred on the left (northwest) flank of the cluster, propagation resulting in its movement toward left of and faster than the movements of the cells. However, in another example of a left-moving multicellular storm, analyzed by CHARBA and SASAKI [18], the contribution of discrete propagation was comparatively small; long-lasting persistent cells, moving strongly to left of the mean wind, dominated (suggesting continuous propagation; see also [6] for a theoretical discussion of the same example in terms of the influence of storm rotation).

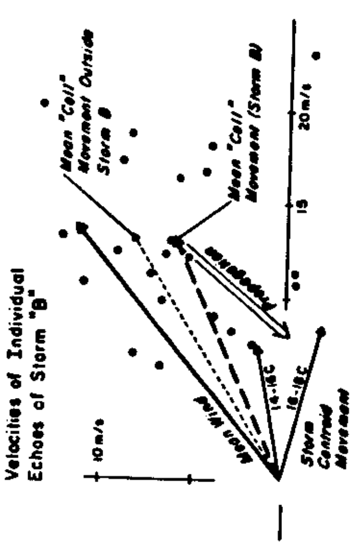

Figure 8
Circles are at endpoints of vector velocities of individual cells in storm *B*. Other features are identified in figure.

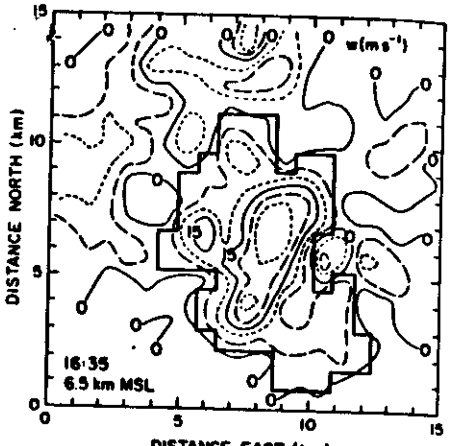

Figure 10.22 Vertical air motion (stippled for w > 9 m s⁻¹) in the active region at 6.5 km MSL at 1635 MDT (without Hanning filter). Heavy line encloses what is called the main updraft at this height.

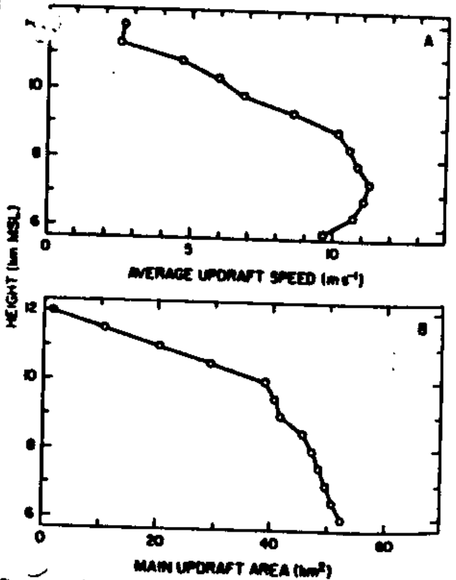

Figure 10.23 Average updraft speed (a) and area (b) for the main updraft at 1635 MDT, as a function of height.

5

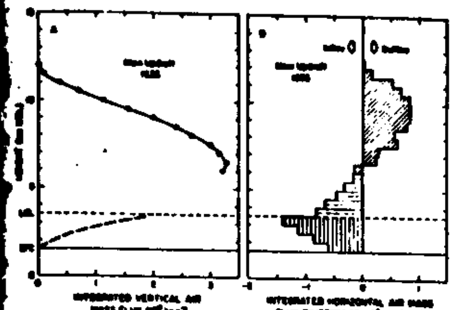

Figure 10.24 (a) Horizontally integrated vertical air mass flux in the main updraft at 1635 MDT. Solid line connects Doppler estimates. The value at cloud base (LCL) is derived from aircraft measurements there. (b) Integrated horizontal air mass flux divergence associated with (a). The vertically hatched portion below cloud base is based on data of Fankhauser (1974) shown in Fig. 10.25. Horizontal hatching indicates subjective interpolation. Errors and further details are discussed in the text.

measurements of flux or flux divergence below 6 km in the main updraft. We speculate, however, about the shape of the D_m profile in the lower levels as follows. Figure 10.25 shows estimates of integrated horizontal air mass flux divergence obtained by Fankhauser (1974) for the subcloud layer of a hailstorm observed in the NHRE area on 9 July 1973. This storm was of comparable size and intensity to the 22 July 1976 storm, and has been discussed at some length in the literature (see, for example, the series of papers summarized by Browning et al., 1976). Measurements of horizontal winds and thermodynamic variables from surface instruments and from three stacked aircraft that circumnavigated the storm were used by Fankhauser to estimate the horizontal flux divergences associated with updraft and downdraft branches of the storm, with air being assigned to updraft and

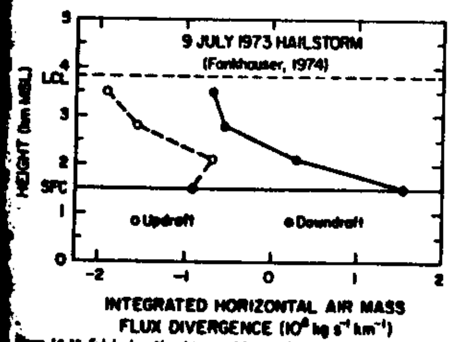

Figure 10.25 Subcloud profiles of integrated horizontal air mass flux divergence. The measurements were obtained during aircraft circumnavigations of a different hailstorm by Fankhauser (1974).

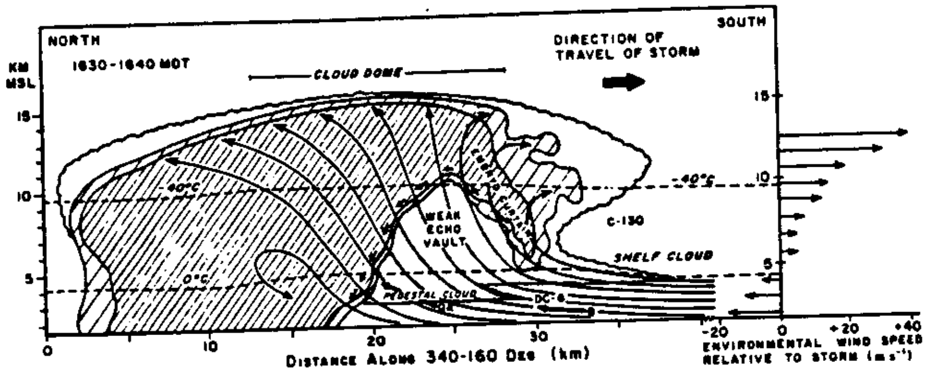

Figure 14.--Vertical section through supercell thunderstorm in northeast Colorado. The section is oriented along the travel direction of the storm, through the updraft core. Two levels of radar reflectivity are represented by different densities of hatched shading. Areas of cloud devoid of detectable echo are shown stippled, the largest such area being the radar vault. The thin lines are streamlines of airflow relative to the storm based on aircraft measurements (thick arrows) and other observations. To the right of the diagram is a profile of the wind component along the direction of travel of the storm as derived from a sounding 50 km south of the storm. The short thin arrows skirting the vault represent a limiting hailstone trajectory (Browning and Foote, 1976).

actual updrafts, apparently forgetting there is a lag between initial condensation in the updraft and development of radar-detectable precipitation. However, Browning and Ludlam (1962) and Browning and Donaldson (1963), noting ... inter-

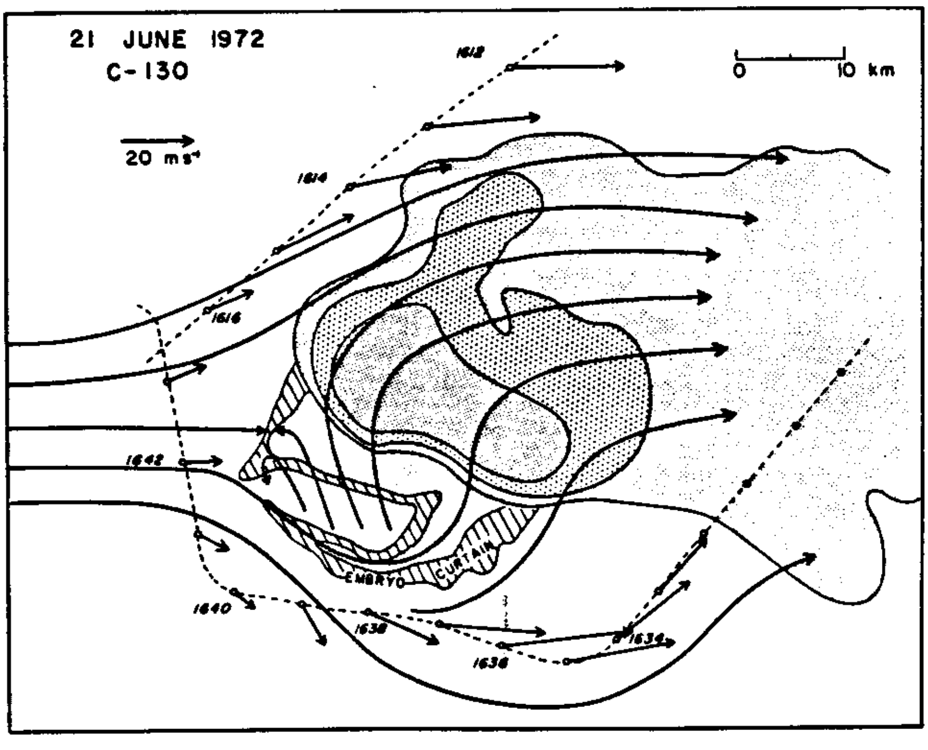

Figure 8.--Thunderstorm updraft behaving as obstacle to strong environmental flow in middle troposphere. Airflow is at 7.9 km MSL around a supercell storm in northeast Colorado. The shaded areas represent different levels of radar reflectivity, the dashed line represents the track of a research aircraft circumnavigating the storm, and the solid

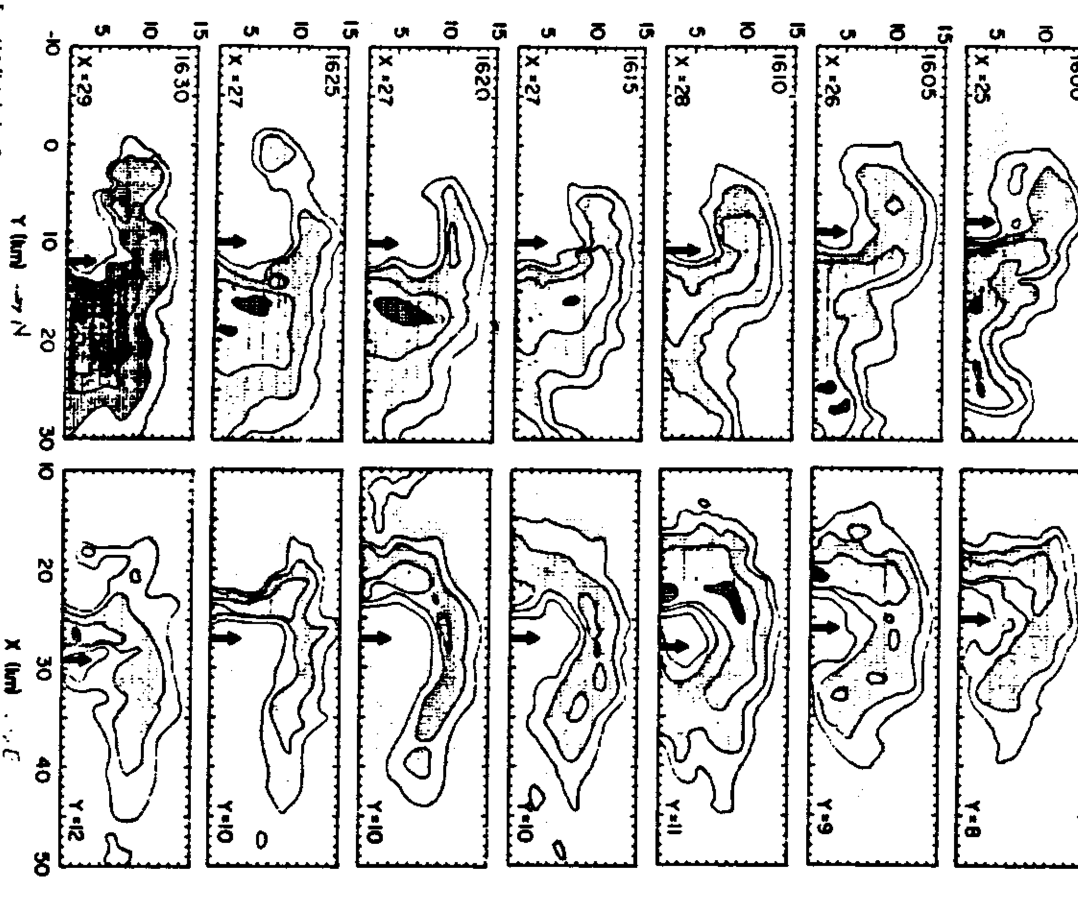

Figure 13.8 Vertical radar reflectivity cross sections demonstrating the persistence and stationarity of a weak echo vault during the 30-min period shown. At each time the x-z (right) and y-z (left) planes are chosen so as to intersect at or near the point (vertically pointing arrow) of the vault's highest penetration. Reflectivities ≥ 20 dBZ$_e$ are shown, but contours are drawn at 10-dB intervals only for reflectivity ≥ 30 dBZ$_e$ to emphasize suspended echo "overhang" in sectors south and east of the vaulted region.

1.1 AIRFLOW MODEL

The circulation of air in and around the Westplains storm s been discussed extensively in the previous four chapters. nce the field of air motion forms the basis for the hail owth calculations to be presented here, it is appropriate to view the basic structure. Figure 20.1 shows in perspective ew the main branches of the circulation. The drawing is

cyclonic vorticity in the updraft. While the updraft itself possess yclonic rotation, individual streamlines (for example, the edges of the updraft ribbon shown) actually turn anticyclonically, as discussed in Chapter 18. Klemp et al. (1981) have illustrated the same phenomenon in cloud model and multiple-Doppler results.

On the shoulders of the updraft the horizontal momentum

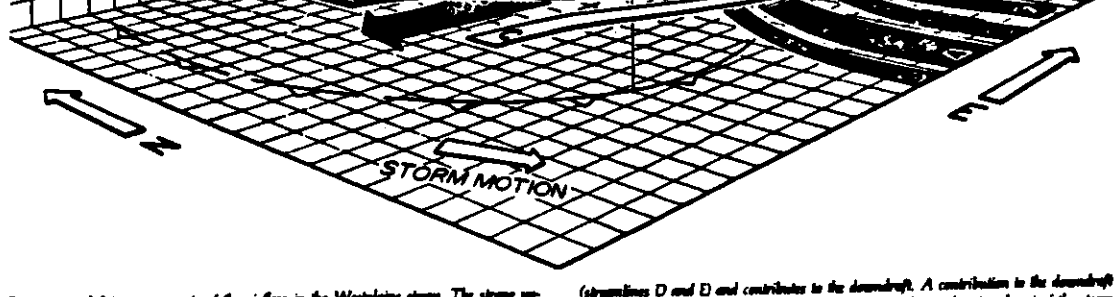

Figure 20.1 Major components of the airflow in the Westplains storm. The strong updraft is depicted by the ribbon labeled A, which starts in the low levels to the south-southeast of the storm, rises sharply in the storm interior, and leaves the storm toward the northeast to form the anvil outflow. On the flanks of the strong updraft the air rises more slowly and penetrates farther to the rear of the storm before also turning to the northeast. In the middle levels there is a tendency for the westerly environmental flow to be diverted, around the sides of the storm (streamlines labeled C) but some air also enters the storm (streamlines D and E) and contributes to the downdraft. A contribution to the downdraft flux is also made by air originally in the low levels to the southeast and east of the storm (streamlines F and G), which then rises several kilometers before turning downward in the vicinity of the echo core. The small circles indicate the computed trajectory of a hailstone, discussed later. The various streamlines are depicted relative to the storm, which is moving toward the south-southeast as shown, rather than relative to the ground.

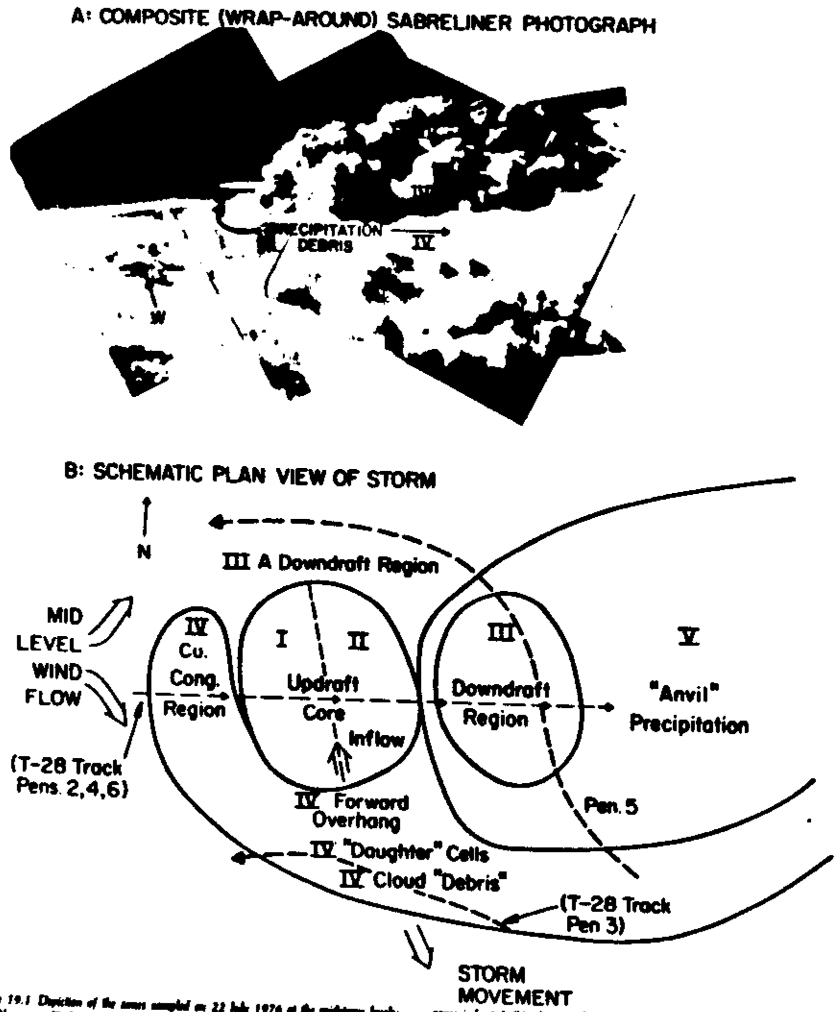

Figure 19.1 Depiction of the zones sampled on 22 July 1976 at the midstorm levels: (a) "Wraparound" photograph taken from the NCAR Sabreliner at 1653 MDT with zones indicated. (b) schematic depiction of zones in (a) in a plan view. Approximate positions of T-28 penetrations relative to main updraft core are indicated.

altitude are given in Fig. 19.2 to show their staged development at the time of penetration. As indicated by the data obtained in the "weak echo" regions (Z_{min}) associated with each of these updrafts, the patterns of reflectivity development differed between cells. Cells I (penetration 2) and K1 (penetration 4) developed in regions of pre-existing, relatively high reflectivity. As these cells developed, each weak echo region (WER) initially became more distinguishable, and then

...ces of 400 m, the percent-
...s and sizes observed* within
... 55 dBZ_e was determined (Fig.
...t into the relationship between
... ar... 'zes and the reflectivity has
... data, hereafter referred to as
... At radar reflectivities below
...egates (> 0.5 mm) were the most
...s (Fig. 19.11c), far outnumbering
...s > 0.5 mm (Fig. 19.11a,b). Small
...graupel particles (≈ 0.5 mm) were
...gions, although less frequently.
... the observed particles tended
...ere more heavily rimed than at
...e regions, rimed aggregates and
...m) were the most commonly
...11d-e). The dip in the observed
...tes in the 30-40 dBZ_e range coin-
...updraft core (WER); in this reflec-
...s were predominant. As the radar
... 40-55 dBZ_e range, the observed
..., rimed particles including large
...1e) and large, rimed aggregates;
...s were observed. The frequency
...h size (Fig. 19.11e) observed in the
...ilar form to that inferred for
...wavelength-radar hail signals (i.e.,
...1976 (Jameson and Heymsfield,

...scription of radar-particle habit
...where in the middle levels of the
...nstruct an approximate composite
... the position of the main updraft

...onsidered when applying this figure toward
...cles at a location for radar reflectivity data. One
...d between the sampling volumes of the probes
...bability curves for planar crystals and aggregates
...used for graupel particles and hail (foil impactor
...spect is that large aggregates (> 1.0 cm) would
...he sampling volume threshold of the 2-D probe,
...detected. The third aspect is that there are also
...tween the radar and the aircraft probes.

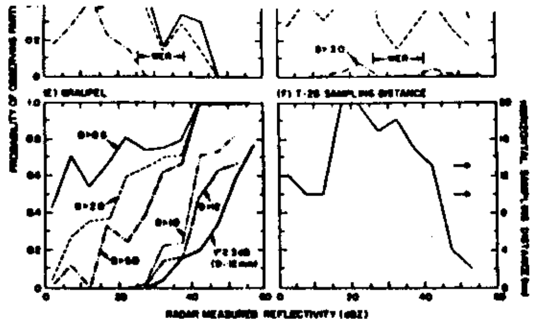

Figure 19.11 Curves relating the frequency of observing indicated particle habits and sizes at the indicated radar reflectivities based on the in situ aircraft measurements and radar data. Horizontal distance over which the T-28 sampled in each 5-dBZ_e reflectivity range is indicated (f). Data obtained in the weak echo regions are in the reflectivity range indicated by WER in C and D.

core at the midstorm level (Fig. 19.12) during the observational period, assuming a degree of steadiness in the reflectivity and wind field patterns, the conditions for which were nearly met during the observational period (see Chapters 16 and 18).

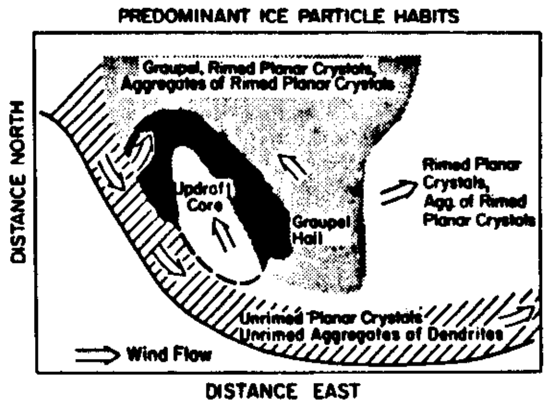

Figure 19.12 Summary of observed ice particle habits in the middle level of the storm, based upon the correlation between radar echo intensity and habit. Predominant windflow in each region is indicated.

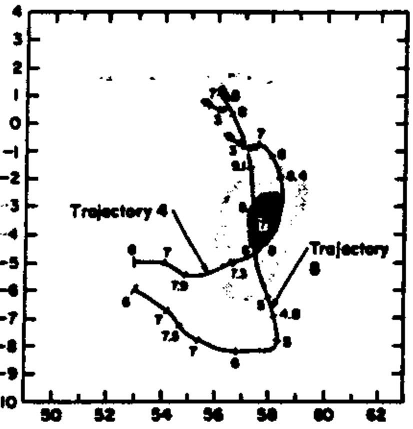

…ure 20.12 Trajectories 4 and 8 in plan view, similar to Fig. 20.9. Heights (km MSL) … indicated along the tracks. Both trajectories are initiated with 2-mm embryos at … km MSL, and the only difference is the initial 1-km separation in the horizontal.

…e hail growth model proposed by Browning and Foote (1976). Fig. 20.13 shows its trajectory in north-south vertical …ection. Unlike trajectories 1-3, it experiences a large excur…ion in the vertical. Indeed, if all hail trajectories were similar …o number 8, one would expect the storm's radar echo to …isplay a large vault. The vault in the present storm is not …ery large and is quite transitory (Chapter 16). In spite of …ssing through the updraft maximum, this trajectory does … lead to very large hail: only 0.8 cm in diameter, as … to 1.9 cm for trajectories 1-3. It is of interest to co…

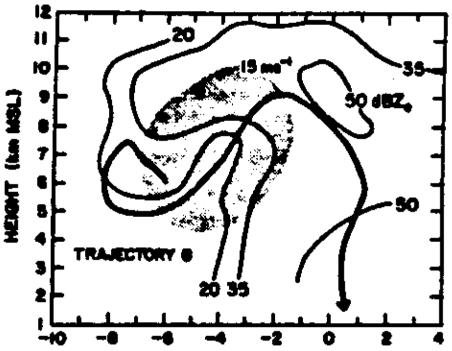

Figure 20.13 Trajectory 8 projected onto a north-south vertical section, as in Fig. 20.10. Unlike trajectories 1 to 3, trajectory 8 experiences a large excursion in the vertical because of the smaller hailstone size upon entering the strong updraft.

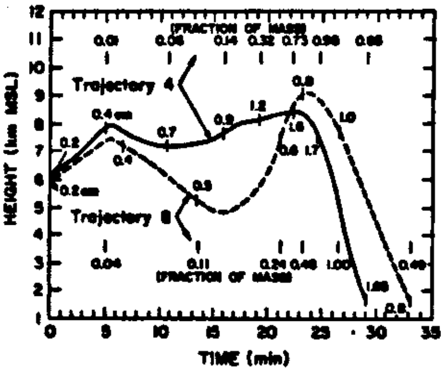

Figure 20.14 Trajectories 4 and 8 in time-height section, and with the hailstone size and mass indicated as in Fig. 20.11.

significantly smaller growth rate than for trajectories 1-4, and

horizontal position (53 km, −3 km) and with the sa… bryo size (2 mm), but at altitudes of 6 and 5 km respe… With reference to Fig. 20.8 and Table 20.1, trajectory … higher altitude moves eastward into the updraft co… leads to hail 1.7 cm in diameter. Trajectory 9 at the … altitude experiences at all times somewhat smaller … speeds and stronger southerly velocities. Though it al… to over 8 km, it stays well to the west of the updraft co… grows to only 0.8 cm.

Trajectories 5 and 6 are started at the same horizont…tion and the same altitude, but with embryo sizes of … 0.4 cm, respectively. They grow to about the same fi… of 1.1 to 1.2 cm, but trajectory 5 accomplishes … moving at relatively constant altitude into the souther… of the updraft, and remaining on the west side of the … core. In contrast, the smaller embryo of trajectory … sharply to an altitude of almost 9 km in passing o… southern part of the updraft, where it accumulates mo… growth. Having diverged by 3-4 km from its compan… ticle on trajectory 5, it then sinks on turning to the no… and passes through the lower region of the updraft … falling to the surface.

The calculated positions (based on the starting co… previously discussed) at which hailstones reach the … are summarized for embryo sizes of 0.4 and 0.8 cm … 20.15 and 20.16. For ease of plotting, the final hailsto… are shown in units of millimeters. For both embryo si… notable result is the strong tendency for the hail to fal… the strongest part of the echo (> 50 dBZₑ). Such a relat… between reflectivity and hailfall has, in fact, been ol… for the Westplains storm, as described in Chapter 1… degree of coincidence between the observed high refl… and hailfall predicted here is surprisingly good, and … regarded as supporting the consistency of the derive… field, the hail growth calculations, and the indep… reflectivity measurements.

While hail predicted to be co-located with the lo… echo core can arrive from a variety of starting lo… because of the strong convergence into the downdr… Chapter 18), the particles seen in the southeast exte… the echo in Figs. 20.15 and 20.16 grow predominantl… trajectories like numbers 8, 10, and 11 of Fig. 20.8, … they fall to the ground somewhat earlier.

Little if any size sorting is evident in the hailfal… with the exception that the largest hail, of 8-, 9-, and …

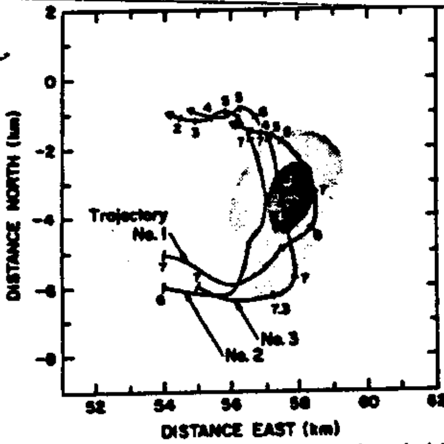

Figure 20.9 Plan view of trajectories 1, 2, and 3 relative to the 15 and 25 m s⁻¹ updraft contours, as in Fig. 20.8. These are examples of trajectories that produced the largest hail. Heights are indicated alongside the tracks in units of kilometers above mean sea level.

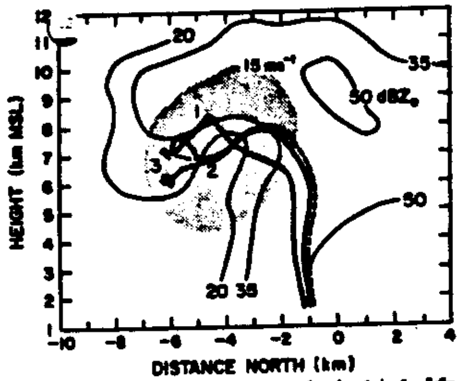

Figure 20.10 Trajectories 1, 2, and 3 projected onto a north-south vertical section. Reflectivities are shown at three levels of intensity for a north-south plane passing through the updraft maximum. The region of updraft exceeding 15 m s⁻¹ in this same plane is also indicated. After entering the updraft from the south, the hailstones grow while making a simple traverse to the north, falling out in the vicinity of the radar echo core.

TABLE 20.1
Hailstone growth histories of 11 …

Trajectory	Embryo diameter	Final diameter	Elapsed time
	(cm)	(cm)	(min)
1	0.6	1.9	22.5
2	0.8	1.9	23.0
3	0.8	1.9	20.7
4	0.2	1.7	20.0
5	0.8	1.2	18.3
6	0.4	1.1	21.0
7	0.8	0.9	23.9
8	0.2	0.8	32.0
9	0.2	0.8	23.9
10	0.2	0.6	32.0
11	0.4	0.5	24.0

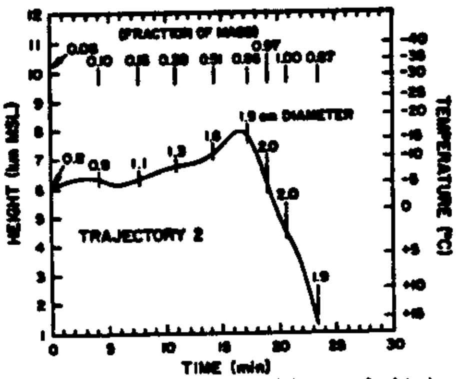

Figure 20.11 Trajectory 2 in time-height section. The hailstone size is indicated at various times along the curve. In the upper part of the figure the mass of the hailstone is represented in terms of its ratio to the maximum mass attained before any melting occurs. In this case 50% of the hailstone mass is accreted in less than 7 min. About 13% of the mass is lost through melting during fallout.

13

MILLER 1985 IRSEE CONF.

20-30 km swath of hail 8-10 cm ϕ max.
1-3 cm ϕ TYPICAL

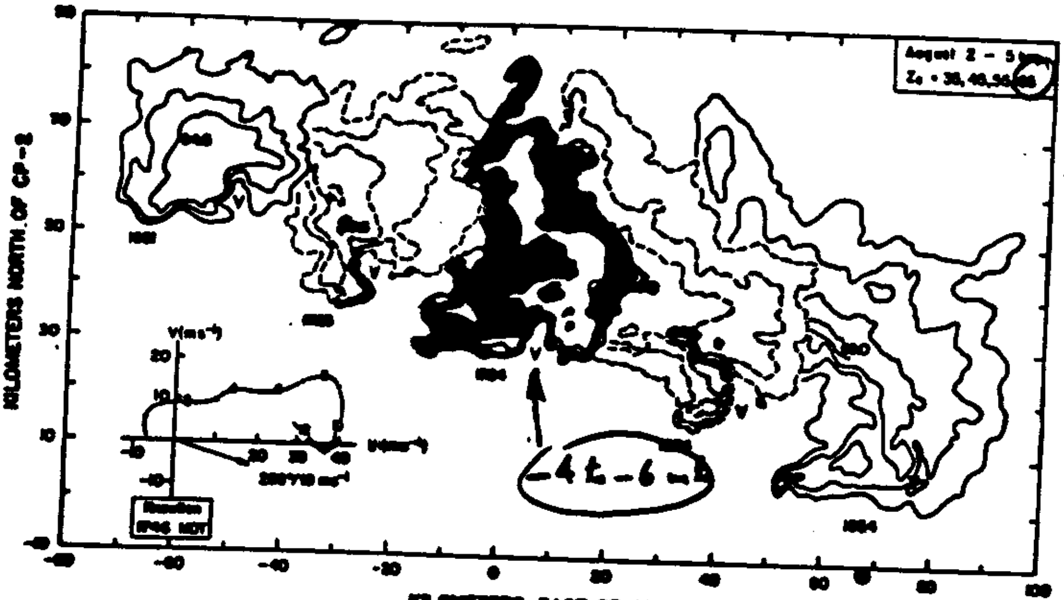

Figure 1 Middle level sections of radar reflectivity (contour interval = 10 dB, starting at 35 dBZ) at the times indicated illustrate the movement of the hailstorm that occurred on 2 August 1981 during the CCOPE in southeastern Montana. Maximum values of reflectivity and the vault (V) are marked. Environmental winds obtained from a tropospheric sounding released at Knowlton (K near x,y=68,-10 km) about 90 km ahead of the storm revealed that the winds veered 90° in the low levels, and there was about 6 x 10^{-3} s^{-1} windshear magnitude from the surface to the level of maximum updraft at 8 km MSL.

14

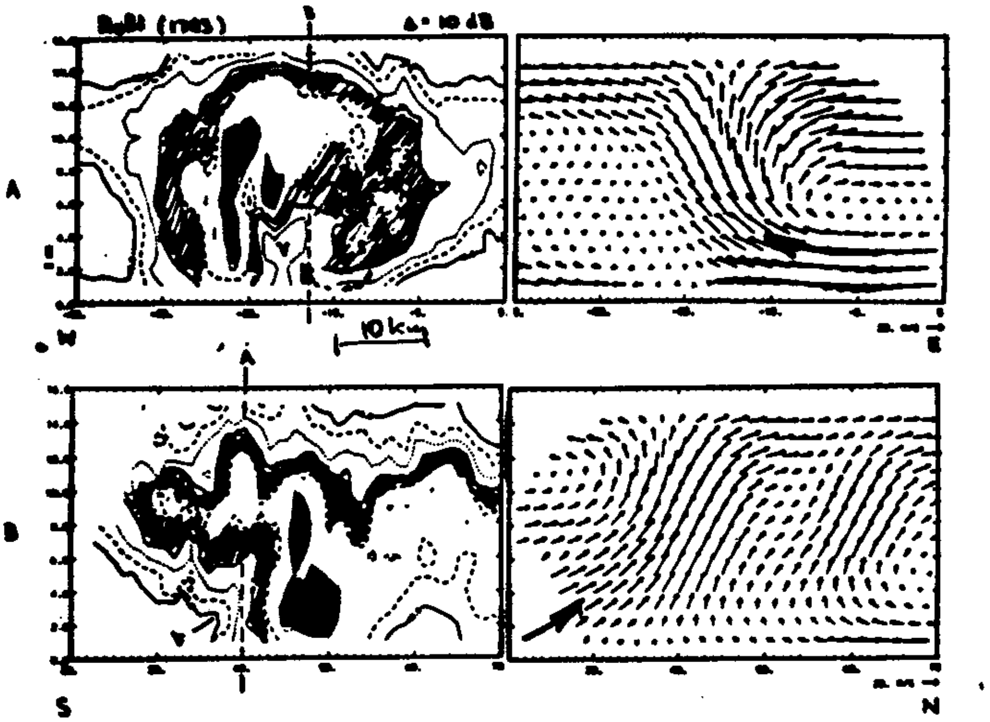

Figure 5 Vertical sections along lines A and B in Fig. 3 of reflectivity (contour interval = 10 dB) on the left and relative flow in these planes on the right. The vault (V) and streamer (S) are shown. Low level air entered the storm's updraft from the east and was exhausted into the anvil, mostly toward the east and north. Though not clearly shown in this section, downdraft air entered the west side of the storm and descended in the western portion of the high reflectivity zone, forming the cold air outflow at the surface.

15

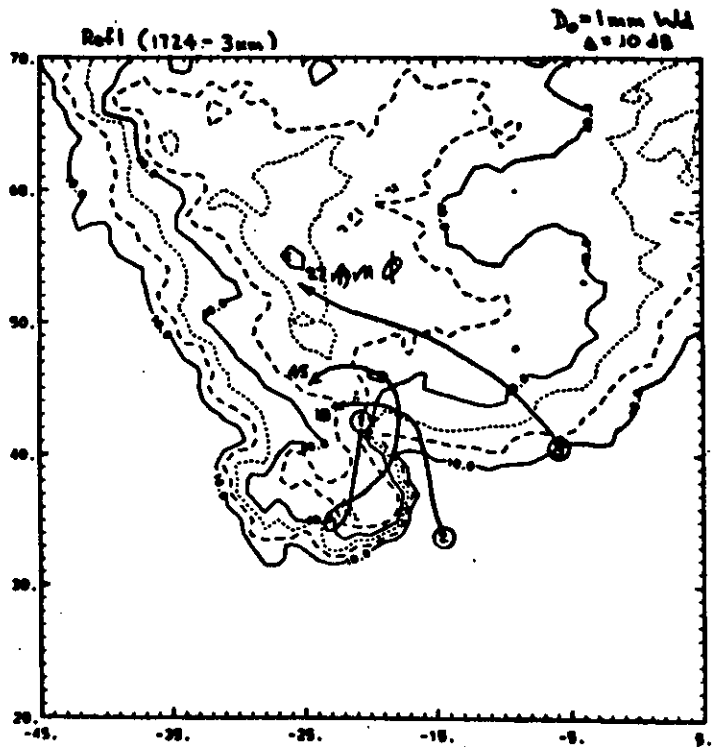

Figure 6 Projections of three hail growth trajectories onto the horizontal plane of reflectivity (contour interval = 10 dB) at 3 km. One-millimeter diameter water drops were started at the locations marked by circled numbers 1, 2, and 3, rose and froze in the updraft near 6 km, passed across the updraft axis (except particle 1 which moved along the major axis of the updraft), and fell out as hail with the indicated diameters (mm).

2 Aug 1981 Supercell

MODEL RESULTS (Preliminary)

1) CSU (Cotton - Tripoli) Regional Atmospheric Modelling System - CRAMS

3D, NON-HYDROSTATIC

FULL $\mu\Pi$: water, ice, graupel mixing ratio
aggregates
ice concentration

Initialized by convergence and temperature anomaly for first 30 min.

First 1½ hr:

- 17 ms^{-1} movement to E ✓
- 42-47 ms^{-1} updraft (55-60 ms^{-1} peak) ✓
- 60-70 dBZ ✓

After 1½ hr: precip. from overhang cuts off inflow, new cell develops to E ✗

∴ $\mu\Pi$ not well modelled, initialization not well observed in boundary layer.

② Terminal Area Simulation System TASS
(Proctor)

3D
62 x 62 grid of 1 km, 32 layers
Orville - Farley microphysics

Location of hail to NW of updraft ✓
Hail reaches the ground after 3 hrs ✗
Surface pressure low 1.5-2.5 mb ≈
(Only one experiment run.)

③ SDSMT (Orville)
2D

Horizontal dimensions too small, multicell rather than supercell character. ✗

Wmax, LWC as observed ✓
Large hail produced ✓

④ Garandi - Zoltan
1D - no precip or hail can fall against the updraft ✗